Available online at www.sciencedirect.com

ScienceDirect

Computational Materials Science 00 (2015) 1–8

Comp. Mat. Sci.

Article

Dopants and dopant–vacancy complexes in tetragonal lead titanate: A systematic first principles study

Paul Erhart[a,*], Karsten Albe[b,**]

[a]Department of Applied Physics, Chalmers University of Technology, S-412 67 Gothenburg, Sweden
[b]Institute of Materials Science, Fachbereich 11, TU Darmstadt, Jovanka-Bontschits-Straße 2, 64287 Darmstadt, Germany

Abstract

A systematic investigation of dopants in tetragonal lead titanate is presented by screening elements from the third period including K, Ca and all 3*d* transition metals. Formation energies and equilibrium transition states are determined by means of density functional theory calculations for both cation sites in the perovskite lattice, which allows us to discriminate between donor and acceptor type behavior. The stability of defect dipoles is determined by calculating the binding energy of transition metal-vacancy complexes. The results reveal that the tendency to substitute the Pb-site rather than the Ti-site monotonically increases going from Ti to Zn. The transition from Ti to Pb substitution depends both on the chemical equilibrium conditions and the position of the Fermi energy. This is most evident for Sc and Zn dopants that in principle can occupy both Pb- and Ti-sites depending on preparation conditions. Except for V all acceptor dopants form defect complexes with oxygen vacancies and thus can form defect dipoles causing hardening as well as aging effects. Defect dipoles involving Pb substitution and oxygen vacancies are found to be unfavorable for all dopants considered here.

Keywords: degradation, electrical and mechanical loading, defects, doping, PZT

1. Introduction

Ferroelectric materials exhibit a spontaneous electric polarization, whose direction can be switched by an applied electric field. Upon cooling from the sintering temperature ferroelectric ceramics undergo a phase transition from a paraelectric to a ferroelectric state, leading to the formation of domains. These domains can be reoriented by poling and result in a remanent polarization as well as dimensional changes of the ceramic [1]. Ferroelectric materials are used in transducers, filters, sensors, ultrasonic motors or actuators [2–6], but also in microelectronic devices like non-volatile ferroelectric memory components [7, 8].

From a commercial point of view, the most important ferroelectric material is lead zirconate titanate (PZT), which is a solid solution of ferroelectric lead titanate and anti-ferroelectric lead zirconate. PZT exhibits a strong piezoelectric response for compositions around the morphotropic phase boundary because of the diverging piezoelectric coefficients [1]. Technically used PZT solid solutions are always doped. Dopant type and concentration determine the piezoelectric properties and influence aging as well as fatigue [9, 10]. They also affect the position of the morphotropic phase boundary and the Curie temperature [11]. In acceptor doped materials Pb or Ti/Zr ions are substituted by ions with a lower valency. In this case, charge neutrality is typically obtained by compensating oxygen vacancies. Acceptor doped materials, which are also referred to as hard doped, are difficult to polarize, exhibit high coercive fields as well as small strains and are thus typically used in sensor applications. Donor doping is realized by the substitution on cation sites with ions of higher valency and typically is associated with the formation of lead vacancies [12]. Soft or donor doped materials can be more easily poled, exhibit higher strains and low coercive fields, whence they are typically used in actors [1]. Technical PZT compositions have typically both acceptor and donor doping to meet the requirements of a given application.

It is well established that in acceptor doped materials defect reactions between dopant and oxygen vacancies can occur. For the prototypical ferroelectric $BaTiO_3$ it was demonstrated

*Corresponding author: erhart@chalmers.se
**Corresponding author: albe@mm.tu-darmstadt.de

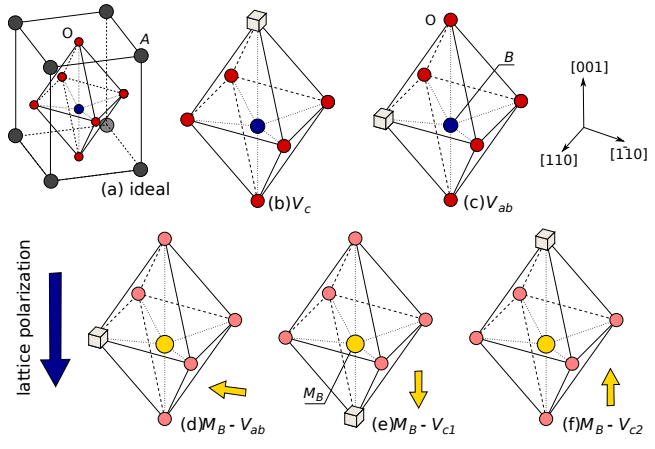

Figure 1. Oxygen vacancy related defect configurations in a tetragonal perovskite lattice structure. (a) Unit cell of a tetragonal perovskite (ABO_3) lattice. (b-c) Vacancy positions. Note that vacancy configurations along the *c*-axis in the undoped unit cell are equivalent, while this symmetry is broken in the presence of dopant atoms. (d-f) Possible configurations for the dipole-acceptor associate with the defect dipole aligned (d) perpendicular, (e) parallel, and (f), anti-parallel to the direction spontaneous polarization.

by electron paramagnetic resonance measurements (EPR) more than three decades ago [13] that $(Mn''_{Ti}-V_O^{\bullet\bullet})^{\times}$ associates are present in reduced crystals, having an excess orientation parallel to the spontaneous polarization [14–16]. Also in lead based perovskites defect complexes, such as $(Cu''_{Ti/Zr} - V_O^{\bullet\bullet})^{\times}$ [17, 18] and $(Fe'_{Ti/Zr} - V_O^{\bullet\bullet})^{\bullet}$, were identified by electron spin resonance (ESR) data and electronic structure calculations [19–25]. These impurity-vacancy associates as well as di-vacancies carry a dipole moment [26]. In tetragonal $PbTiO_3$ acceptor-vacancy associates can assume two different arrangements with respect to the direction of the spontaneous polarization. Oxygen vacancies in one of the four equatorial positions of the oxygen octahedra generate defect dipoles perpendicular to the spontaneous polarization, whereas $V_O^{\bullet\bullet}$ in the apical oxygen positions form defect dipoles collinear to the orientation of spontaneous polarization. Identical arrangements were also found in (La,Fe) co-doped PZT [27]. Non-switching defect dipoles impose a restoring force for reversible domain switching [28]. The presence of acceptor-vacancy defect associates is thus considered the main cause for hardening in PZT ceramics. Since their gradual reorientation is determined by the barrier for oxygen vacancy migration, these defect complexes cannot immediately follow the polarization switching [29].

While there is no doubt about the existence of vacancy-acceptor pairs at ambient conditions, much less is known about their thermodynamic stability. Temperature dependent ESR measurements on Fe-doped $SrTiO_3$ [30] revealed that iron-vacancy associates have a binding energy of -0.22 eV and dissolve at elevated temperatures, which was also found in a recent theoretical study on doped $SrTiO_3$. [31].

For $PbTiO_3$ binding energies have been calculated for complexes of Cu''_{Ti} with oxygen vacancies for various positions (see Fig. 1) [22, 29]. Vacancies in the first neighbor shell of the dopant have binding energies in excess of −0.5 eV. Thus, the dissociation reaction $(Cu''_{Ti} - V_O^{\bullet\bullet})^{\times} \rightleftharpoons Cu''_{Ti} + V_O^{\bullet\bullet}$ is fully on the left hand side at ambient conditions.

The ability to observe the presence and alignment of defect dipoles in ferroelectrics by EPR has had a pronounced impact on the understanding of doping and materials degradation over time. Many dopants are, however, no detectable in EPR measurements and a direct quantitative analysis of defect concentrations and mobilities is experimentally challenging. Thus, in the search of new or alternative dopants one has to rely on intuition and/or empirical rules. If *a-priori* assumptions have been made on defect positions, oxidation states and neutrality conditions, the defect chemistry of perovskites can be discussed in the framework of the Brouwer approximation [32, 33]. Similarly, the treatment of defect chemistry in complex oxides by means of atomistic models using classical interatomic potentials is possible (see e.g., Refs. [34–36]), but does not allow to describe the coupling of the defect's charge state to the Fermi energy in the respective material.

However, with the advent of accurate and efficient electronic structure methods that allow the calculation of defect formation energies of individual, differently charged defect configurations, a conceptually more fundamental approach is available for addressing the problem of defect equilibria in metal oxides (see e.g., Refs. [37–42]).

In this paper, we investigate the full series of 3*d* transition metals as dopants in $PbTiO_3$ and also consider the 4*s* elements K and Ca from the first and second group of the same period. Based on electronic structure calculations within density functional theory, we calculate formation energies of differently charged states of dopants on A and B-sites of the perovskite lattice, determine equilibrium transition levels, as well as association energies of vacancy-dopant complexes.

2. Methodology

2.1. Total energy calculations

Calculations were carried out within density functional theory as implemented in the Vienna ab-initio simulation package [43–46]. The ion cores and core electrons were described using the projector augmented wave method [47, 48]. For transition metals semi-core states were explicitly included. The plane-wave energy cutoff was set to 500 eV. The exchange-correlation potential was represented using the local spin density approximation (LSDA). [1] All defect calculations were carried out at constant volume using $2 \times 2 \times 3$ supercells (60 atoms in the ideal cell). Brillouin zone integrals were evaluated using a non-shifted $4 \times 4 \times 4$ Monkhorst-Pack mesh.

2.2. Defect formation energy

Defect formation energies were obtained using [49]

$$\Delta E_D = (E_D - E_H) - q(\varepsilon_{\mathrm{VBM}} + \mu_e) - \sum_i \Delta n_i \mu_i, \qquad (1)$$

[1] For many materials the spin-polarized generalized gradient approximation is superior to the LSDA. In the case of ferroelectric perovskites, however, it has been repeatedly observed that the LSDA yields better agreement with experiment with respect to structural and ferroelectric properties.

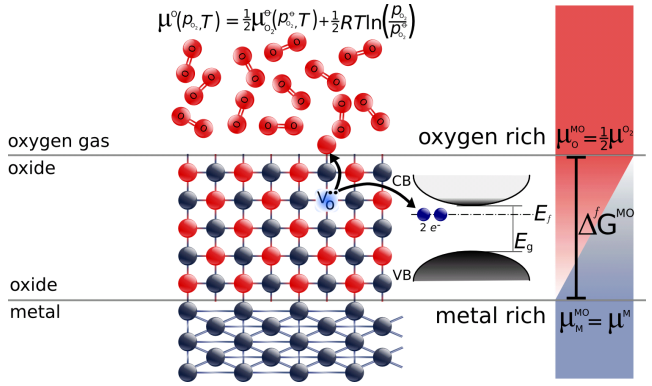

Figure 2. The chemical potentials of the constituent elements depend on the chemical environment. The oxygen chemical potential μ_{O_2} in particular varies with oxygen partial pressure p_{O_2} and temperature as described by the relation at the top of the figure. The chemical potentials of the constituents are coupled by the condition that their weighted sum equal the free energy of formation ΔG^{MP} as graphically illustrated on the right hand side. In materials with a band gap defect formation usually also involves the exchange of electrons or holes with the electron reservoir, which is thermodynamically represented by the electro chemical potential μ_e. Also compare Eq. (1).

where μ_i is the chemical potential of component i. Here, Δn_i denotes the difference in the number of atoms of element i between the cell with and without the defect, e.g., for an isolated oxygen vacancy $\Delta n_O = -1$ whereas all the other Δn_i are zero. E_D is the total energy of the supercell containing the defect and E_H is the total energy of the ideal reference cell. The defect formation enthalpy is linearly dependent on the defect charge state q and the electron chemical potential μ_e which is measured with respect to the valence band maximum ε_{VBM}.

At this point it is important to note that the chemical potential of each constituent species depends on the thermodynamic environment. If the metal oxide MO is in equilibrium with an oxygen vapor, the chemical potential of every constituent is varying with the oxygen partial pressure and therefore also the defect formation energy (see Fig. 2).

The range of variation of the chemical potentials is, however, restricted by the stability of the phase of interest. Therefore, one can rewrite Eq. 1 by taking into account the difference between the number of atoms of type i in the reference cell with respect to the defective cell Δn_i, respectively. Then the chemical potential μ_i of each constituent i can be rewritten as $\mu_i = \mu_i^{bulk} + \Delta\mu_i$, where μ_i^{bulk} denotes the chemical potential of the standard reference state and is equivalent to the cohesive energy per atom at $T = 0\,\mathrm{K}$.

The supercell approximation introduces systematic errors due to periodic image interactions. The formation energies presented in the following were therefore corrected for potential alignment effects (see e.g., Ref. [50]) using the approach described in Ref. [51]. Image charge interactions were accounted for using the simplified correction scheme outlined in Ref. [50], which is based on a scaled monopole-monopole correction.

The computational parameters used in this work are similar to previous studies (see e.g., Refs. [21, 22, 40, 52]). In comparison with Refs. [22] and [40] the supercells employed in the present study are relatively small. It must be stressed, however, that the objective of the present work is to compare a large number of different impurities in order to reveal systematic trends. The error due to the limited size of the supercells is estimated to be on the order of 0.1–0.2 eV.

The more serious shortcoming of the present approach is the band gap underestimation, which is very well known for LSDA calculations. While in principle hybrid functionals yield band gaps in much better agreement with experiment [53, 54], they are also computationally much more expensive, whence they have not been used in the present context. For consistency in the analysis of the defect formation energies, which according to Eq. (1) depend on the electron chemical potential, only the calculated band gap is used.

Table 1. Bulk properties of oxide phases of the components. ΔH_f: enthalpy of formation (eV/f.u.); a_0, b_0, c_0: lattice constants (Å); B: bulk modulus (GP). Experimental data from References [55–57].

	Experiment	This work
PbO, orthorhombic (Pbcm, sg no. 57, ICSD no. 15402)		
ΔH_f		−3.12
a_0	5.876	5.827
b_0	5.476	5.386
c_0	4.743	4.664
PbO, tetragonal (P4/nmm, sg no. 129, ICSD no. 15466)		
ΔH_f	−2.27	−3.16
a_0	3.96	3.944
c_0	5.01	4.876
PbO_2, orthorhombic (Pbcn, sg no. 60, ICSD no. 20362)		
ΔH_f	−2.88	−4.51
a_0	4.948	5.074
b_0	5.951	5.816
a_0	5.497	5.414
PbO_2, tetragonal ($P4_2/mnm$, sg no. 136, ICSD no. 23292)		
ΔH_f		−4.50
a_0	4.958	4.945
c_0	3.388	3.390
Pb_2O, cubic ($Pn\bar{3}$, sg no. 201, ICSD no. 28838)		
ΔH_f		−1.99
a_0	5.38	5.323
Pb_2O_3, orthorhombic ($Pmc2_1$, sg no. 26, ICSD no. 36295)		
ΔH_f	−5.10	−5.89
a_0	7.78	7.673
b_0	5.49	5.414
c_0	7.64	7.646
Pb_3O_4, tetragonal ($P4_2/mbc$, sg no. 135, ICSD no. 4106)		
ΔH_f	−7.45	−10.98
a_0	8.811	8.708
c_0	6.563	6.614
TiO_2, rutile (I4/mmm, sg no. 139)		
ΔH_f	−9.78	−10.93
a_0	4.594	4.572
c_0	2.959	2.926
Ti_2O_3 ($R\bar{3}c$, sg no. 167)		
ΔH_f	−15.77	−18.10
a_0	5.149	5.439
α	56.6	54.8

3. Phase stability

In a first step the thermodynamic stability limits of $PbTiO_3$ with respect to all possible boundary phases have to be deter-

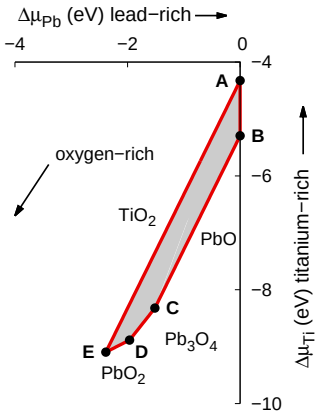

Figure 3. Stability diagram of tetragonal lead titanate constructed on the basis of formation energies from density functional theory calculations. The gray polygon indicates the range of stability of tetragonal lead titanate. The different segments are obtained by imposing all relevant equilibrium conditions. For example, $\overline{AE}$ corresponds to the equilibrium between TiO_2 and $PbTiO_3$, see (4). The data used to construct this diagram is summarized in Table 1.

mined. Equation (1) provides a mathematical expression for the dependence of the defect formation enthalpy on the chemical environment, which enters via the chemical potentials μ_i. The latter cannot be adjusted freely, but are subject to thermodynamic constraints related to the formation of lead titanate as well as various competing phases. Specifically, the reaction equation for the formation of $PbTiO_3$ connects the chemical potentials of Pb, Ti, and O,

$$\Delta\mu_{\mathrm{Pb}} + \Delta\mu_{\mathrm{Ti}} + 3\Delta\mu_{\mathrm{O}} = \Delta H_f[\mathrm{PbTiO_3}], \tag{2}$$

which can be used to eliminate the chemical potential of oxygen $\Delta\mu_{\mathrm{O}} = \frac{1}{3}\left(\Delta H_f[\mathrm{PbTiO_3}] - \Delta\mu_{\mathrm{Pb}} - \Delta\mu_{\mathrm{Ti}}\right)$, where $\Delta H_f[\mathrm{PbTiO_3}]$ denotes the formation energy of lead titanate. For certain values of the chemical potentials of lead and oxygen the formation of lead oxides is energetically more favorable than the formation of lead titanate, which leads to the following set of inequalities:

$$\begin{aligned}
\Delta\mu_{\mathrm{Ti}} &\geq \Delta H_f[\mathrm{PbTiO_3}] - 3\Delta H_f[\mathrm{PbO}] + 2\Delta\mu_{\mathrm{Pb}} \\
\Delta\mu_{\mathrm{Ti}} &\geq \Delta H_f[\mathrm{PbTiO_3}] - \tfrac{3}{2}\Delta H_f[\mathrm{PbO_2}] + \tfrac{1}{2}\Delta\mu_{\mathrm{Pb}} \\
\Delta\mu_{\mathrm{Ti}} &\geq \Delta H_f[\mathrm{PbTiO_3}] - 3\Delta H_f[\mathrm{Pb_2O}] + 5\Delta\mu_{\mathrm{Pb}} \\
\Delta\mu_{\mathrm{Ti}} &\geq \Delta H_f[\mathrm{PbTiO_3}] - \Delta H_f[\mathrm{Pb_2O_3}] + \Delta\mu_{\mathrm{Pb}} \\
\Delta\mu_{\mathrm{Ti}} &\geq \Delta H_f[\mathrm{PbTiO_3}] - \tfrac{3}{4}\Delta H_f[\mathrm{Pb_3O_4}] + \tfrac{5}{4}\Delta\mu_{\mathrm{Pb}}
\end{aligned} \tag{3}$$

Taking into account the oxide phases of titanium, one arrives at yet another set of inequalities:

$$\begin{aligned}
\Delta\mu_{\mathrm{Ti}} &\leq \tfrac{3}{2}\Delta H_f[\mathrm{TiO}] - \tfrac{1}{2}\Delta H_f[\mathrm{PbTiO_3}] + \tfrac{1}{2}\Delta\mu_{\mathrm{Pb}} \\
\Delta\mu_{\mathrm{Ti}} &\leq 3\Delta H_f[\mathrm{TiO_2}] - 2\Delta H_f[\mathrm{PbTiO_3}] + 2\Delta\mu_{\mathrm{Pb}} \\
\Delta\mu_{\mathrm{Ti}} &\leq \Delta H_f[\mathrm{Ti_2O_3}] - \Delta H_f[\mathrm{PbTiO_3}] + \Delta\mu_{\mathrm{Pb}} \\
\Delta\mu_{\mathrm{Ti}} &\leq \tfrac{3}{4}\Delta H_f[\mathrm{Ti_3O_5}] - \tfrac{5}{4}\Delta H_f[\mathrm{PbTiO_3}] + \tfrac{5}{4}\Delta\mu_{\mathrm{Pb}} \\
\Delta\mu_{\mathrm{Ti}} &\leq \tfrac{3}{5}\Delta H_f[\mathrm{Ti_4O_7}] - \tfrac{7}{5}\Delta H_f[\mathrm{PbTiO_3}] + \tfrac{7}{5}\Delta\mu_{\mathrm{Pb}}.
\end{aligned} \tag{4}$$

Knowledge of the formation energies of these compounds thus allows construction of the stability diagram for lead titanate as a function of the chemical potentials of Pb and Ti. Not all of the compounds appearing in Eqs. (3) and (4) are actually relevant since the respective inequalities are overridden by others. An initial assessment based on experimental data identifies the compounds given in Table 1 as the most important ones. For consistency with the defect calculations discussed below the properties of the constituents as well as the compounds involved have been calculated using the computational parameters given in Sec. 2 (with appropriately adjusted $\boldsymbol{k}$-point meshes).[2] The results of these calculations are compared with experimental data in Table 1 demonstrating good overall agreement. The calculated values were employed to construct the stability diagram shown in Fig. 3, which is in good agreement with the diagram based on experimental data. In Fig. 3 five different points (A-E) are indicated, which will be used in the following sections to exemplify the dependence of the defect formation energies on the chemical conditions.

4. Defects

In this section, we first discuss the formation energies of isolated impurities in tetragonal lead titanate that determine the equilibrium concentrations and solubilities, respectively. Subsequently, these data are employed to derive the transition levels which allow us to categorize the various impurities as donors and acceptors. Afterwards the connection between the formation energies and the phase diagram is explored revealing the balance between substitution on Pb and Ti sites. Finally, the association of impurities with oxygen vacancies, which is important in terms of defect dipole formation, is addressed.

4.1. Isolated impurities

Figure 4 shows the formation energies of isolated impurities in lead titanate under impurity-rich conditions ($\Delta\mu = 0$ for the impurity atom type in Eq. (1)). If substituted for titanium K, Ca, and Sc as well as Co, Ni, Cu, and Zn act as acceptors, V acts as a donor, Cr and Fe behave ambipolar whereas Mn is electrically inactive. With regard to lead substitution we find K, Cu, and Ni to exhibit acceptor characteristics while Sc, V, and Mn are donors. Zn and Cr are electrically inactive whereas Co and Fe display ambipolar behavior. The equilibrium transition levels can be deduced from the formation energy plots shown in Fig. 4 and correspond to the location of the symbols in that figure.

Figure 5 shows the formation energies of both (a) titanium and (b) lead substitutional defects as a function of the atomic number. Both for Ti and Pb substitution, the formation energy increases for the $3d$ transition metals to the right of Ti with increasing group number, while the $4s$ elements K and Ca show higher energies than Sc. Note that the calculated formation energies are negative since we assumed impurity rich conditions, *i.e.* the reference state is the respective pure element.

[2] The LSDA is known to provide only a mediocre description of formation enthalpies. The calculation results compiled in Table 1 are representative of the level of agreement that can be achieved.

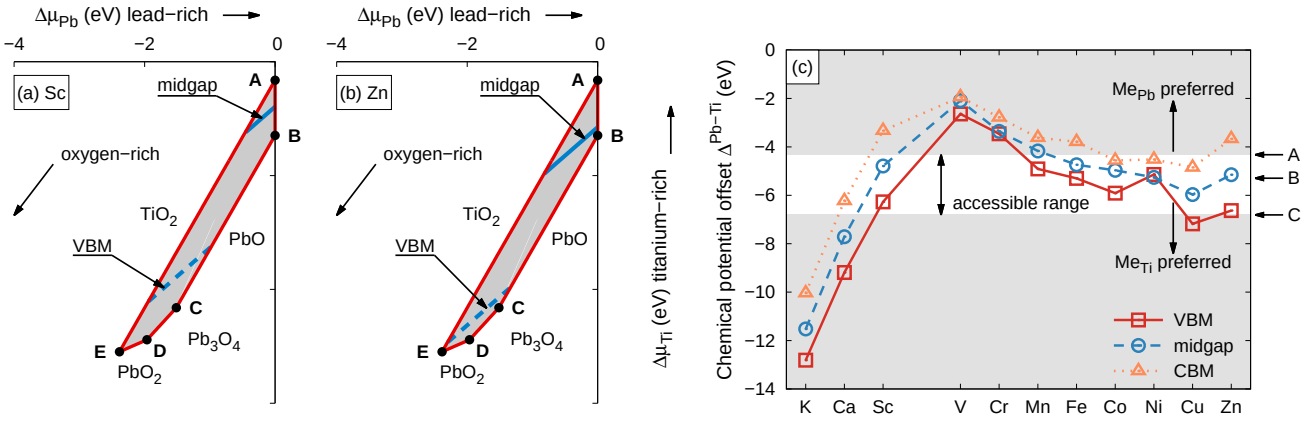

Figure 6. (a,b) Stability diagrams illustrating the balance between titanium and lead substitution for (a) Sc and (b) Mn. Ti substitution is energetically more favorable if the chemical potentials are below the blue lines, whereas Pb substitution is more favorable in the range above the blue lines. The solid, dashed and dotted lines indicate the equivalent information for electron chemical potentials located at midgap, the valence band maximum (VBM) and the conduction band minimum (CBM), respectively. (c) Chemical condition, at which transition from Ti to Pb substitution occurs, as a function of the atomic number. Specifically, the figure shows the difference between the chemical potentials of Pb and Ti. The arrows on the right hand side indicated the respective values for points A through E indicated in (a,b).

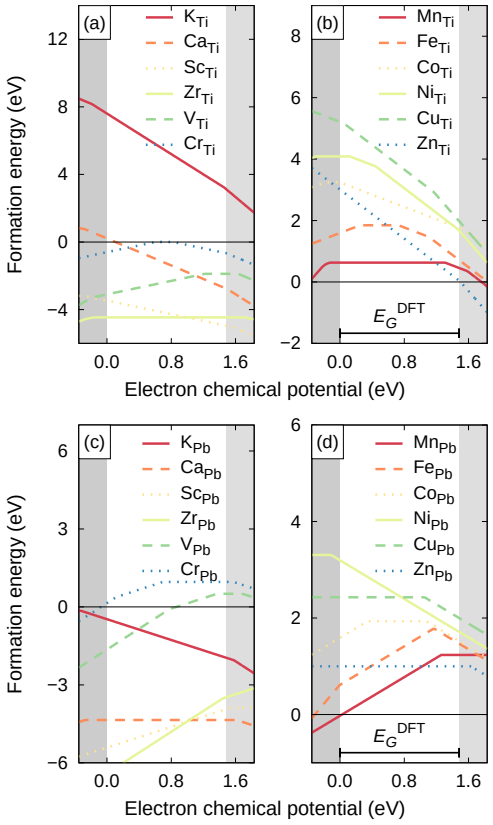

Figure 4. Formation energies of isolated transition metal impurities on (a,b) titanium and (c,d) lead sites using the chemical potentials corresponding to point A in Fig. 3. Changes in slope correspond to equilibrium transition levels.

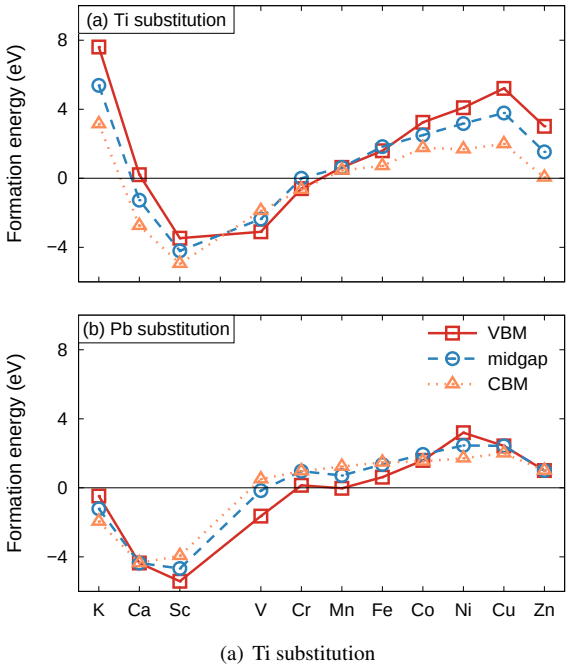

(a) Ti substitution

Figure 5. Formation energies of isolated transition metal impurities when substituted for (a) titanium and (b) lead, respectively. Different colors and line styles are used to indicate the variation of the formation energies across the band gap, compare Fig. 4.

4.2. Balance between Ti and Pb substitution

We can now investigate the balance between Ti and Pb-substitution for individual impurities, *i.e.* we can determine the range of chemical potentials for which either one is dominant. The results of this analysis are summarized in Fig. 6. Figures 6(a,b) show a blowup of the stable region of the phase diagram (compare Fig. 3), where the range within which either Ti or Pb substitution is energetically more favorable, has been indicated. The figure should be read as follows: If the electron chemical potential is located in the middle of the band gap, Ti substitution is energetically more favorable for the range of chemical potentials below the solid blue line, whereas Pb substitution is more favorable in the range above this line. The dashed and dotted lines indicate the equivalent information for electron chemical potentials located at the valence band maximum (VBM) and the conduction band minimum (CBM), respectively. For Sc, with an electron chemical potential at midgap, Ti substitution is thus dominant over roughly two thirds of the accessible range, whereas for Mn it dominates over an even larger range. To characterize the dependency of this range on the atomic number, Fig. 6(c) shows the chemical potential offset $\Delta^{\mathrm{Pb-Ti}} = \Delta\mu_{\mathrm{Pb}} - \Delta\mu_{\mathrm{Ti}}$, at which transition from Pb to Ti substitution occurs. The values of $\Delta^{\mathrm{Pb-Ti}}$ at the points A, B, C, D, and E shown in the phase diagram in Fig. 3 are indicated by the arrows on the right. Comparison with Fig. 5, shows that the dependence of $\Delta^{\mathrm{Pb-Ti}}$ on the atomic number is opposite to the formation energies. We find that for K and Ca almost only Pb substitution should be observed while for V only Ti substitution is possible. The remaining ions display at least some range within which both substitutions can be achieved. Most sensitive to the preparation conditions should be Sc, which depending on the chosen equilibrium conditions, can substitute on either Pb or Ti sites. Thermodynamically, it is thus possible to switch from Ti to Pb substitution. Whether or not this can be achieved in reality depends on the experimental ability to generate Pb *vs* Ti-rich conditions and to reach thermodynamic equilibrium.

4.3. Association between impurities and oxygen vacancies

If an oxygen vacancy forms a defect associate with an impurity metal ion, the resulting complex carries a dipole moment. Electrostatically, substitutional defects should bind to oxygen vacancies only if they carry an effective negative charge, *i.e.* if they behave as acceptors. But as the bonding in lead titanate also exhibits covalent character, the binding energies might also depend on lattice strain and relaxation.

By lattice symmetry, there are three distinct nearest neighbor oxygen vacancy-impurity complexes if the metal ion substitutes on the B-site for Ti as shown in Fig. 1. In the first case ($M_{\mathrm{Ti}} - V_{ab}$), the oxygen vacancy located in the same plane as the metal ion and the resulting dipole vector will point along one of the $\langle 100 \rangle$ directions. In the second case ($M_{\mathrm{Ti}} - V_{c1}$), the oxygen vacancy is located at the nearest neighbor O-site along the [001] direction while in the third case ($M_{\mathrm{Ti}} - V_{c2}$) the oxygen vacancy occupies the nearest neighbor site along the $[00\bar{1}]$ direction. There are four equivalent $M_{\mathrm{Ti}} - V_{ab}$ configurations while the $M_{\mathrm{Ti}} - V_{c1}$ and $M_{\mathrm{Ti}} - V_{c2}$ occur only once each.

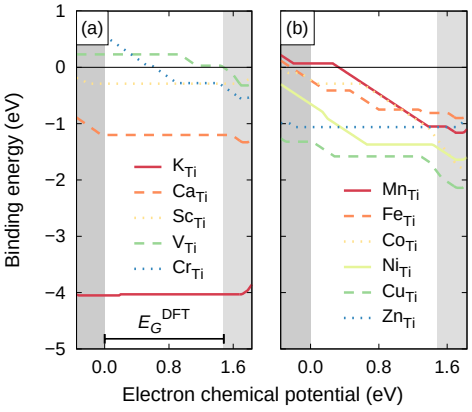

Figure 7. Binding energies of transition metal-oxygen vacancy complexes. Here negative binding energies indicate that complex formation is energetically favorable, which is thus the case for the vast majority of dopants considered here.

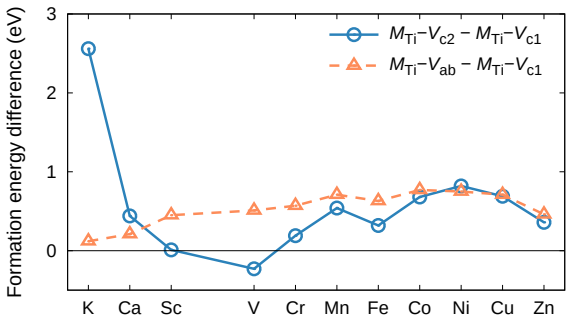

Figure 8. Energy difference between vacancy-dopant associates in various positions The open circles correspond to the energy difference between dipoles oriented anti-parallel and parallel to the spontaneous polarization, triangles show the energy difference between the equatorial position and the parallel alignment (compare Fig. 1).

In Fig. 7, the binding energies for $M_{\mathrm{Ti}} - V_{c1}$ complexes as a function of the electron chemical potential are shown. Except for V and Cr, all energies are negative throughout the band gap and have values of about 0.5 eV and larger. Thus, we can conclude that the formation of dopant-vacancy associates can be expected for all dopants occupying the B-site position at ambient conditions. One can furthermore observe that the binding energy is not constant throughout the gap but exhibits changes in magnitude and slope due to changes in the charge states of the defect complexes and the constituting isolated defects.

In Fig. 8 the calculated energy differences between dipoles oriented anti-parallel and parallel to the spontaneous polarization are shown together with data representing the energy difference between the equatorial orientations ($M_{\mathrm{Ti}} - V_{ab}$) and the parallel alignment ($M_{\mathrm{Ti}} - V_{c1}$). For all dopants that can potentially substitute the Ti-cation, the ($M_{\mathrm{Ti}} - V_{c1}$) position is energetically favored. Only for V and Sc the collinear positions are energetically degenerate. These data can be considered in connection with the analysis of the dipole reorientation kinetics presented in Ref. [29], as the energy differences between ($M_{\mathrm{Ti}} - V_{c1}$) and ($M_{\mathrm{Ti}} - V_{c2}$)/($M_{\mathrm{Ti}} - V_{ab}$) configurations yield a first impression of the energy landscape for defect dipole reorientation. More detailed calculations are, however, required in order to provide quantitative information regarding the dipole kinetics.

Finally, we also investigated the possibility of defect dipole formation between dopants on Pb sites and oxygen vacancies. Each Pb-site has four nearest neighbors in the plane above and four nearest neighbors in the plane below. These bonds are oriented along the ⟨111⟩ directions. The calculations, however, failed to produce any bound configurations for any of the elements considered in this study.

5. Summary

We have investigated doping effects in lead titanate of elements from the third row of the periodic table by means of total energy calculations of defects in different charge states and for various thermodynamic boundary conditions. The results reveal that 3*d*-transition metal dopants exhibit increasing formation energies with increasing group number. The tendency to substitute on the Pb-site rather than the Ti-site is increasing with higher atomic number for elements to the right of Ti, while depending also on chemical boundary conditions and the Fermi level. The latter effect is most evident for Sc dopants that in principle can occupy Pb or Ti-sites depending on preparation conditions. Except for V all acceptor dopants form defect complexes with O-vacancies and thus can form defect dipoles, which can cause hardening but also aging effects.

Acknowledgments

This work has been partly supported by SFB 595 “Electrical fatigue in functional materials”. P.E. acknowledges funding from the “Areas of Advanced Materials Science” at Chalmers, the Swedish Research Council in the form of a Young Researcher Grant and the European Research Council in the form of a Marie Curie Career Integration Grant. Computer time allocations by the Swedish National Infrastructure for Computing at C3SE (Gothenburg) and PDC (Stockholm) are gratefully acknowledged.

[1] B. Jaffe, C. W.R., J. H., Piezoelectric Ceramics, Academic Press, London and New York, 1971.
[2] W. Heywang, K. Lubitz, W. W. (Eds.), Piezoelectricity - Evolution and Future of a Technology, vol. 114 Edition, Springer Series in Materials Science, 2008.
[3] K. Uchino, J. Electroceram. 20 (3-4) (2007) 301–311.
[4] N. Setter (Ed.), Piezoelectric Materials and Devices, Ceramics Laboratory EPFL, Lausanne, 2002.
[5] Y. Xu, Ferroelectric Materials and their Applications, Elsevier, Amsterdam, 1991.
[6] J.-M. Sallese, P. Fazan, Sensors and Actuators A 109 (3) (2004) 186–194.
[7] J. F. Scott, Science 246 (4937) (1989) 1549–1549.
[8] J. F. Scott, C. A. P. Dearaujo, Science 246 (4936) (1989) 1400–1405.
[9] Y. A. Genenko, J. Glaum, M. J. Hoffmann, K. Albe, Mat. Sci. & Eng. B, 192 (2015) 52–82
[10] Y. A. Genenko, O. Hirsch P. Erhart, J. Appl. Phys., 115 (2014) 104102
[11] N. J. Donnelly, T. R. Shrout, C. A. Randall, J. Amer. Ceram. Soc. 90 (2) (2007) 490–495.
[12] R.-A. Eichel, H. Mestric, H. Kungl, M. J. Hoffmann, Appl. Phys. Lett. 88 (12) (2006) 122506.
[13] G. P. V. Jonker, P. V. Lambeck, Ferroelectrics 21 (1-4) (1978) 641–643.
[14] L. Zhang, E. Erdem, X. Ren, R.-A. Eichel, Appl. Phys. Lett. 93 (20) (2008) 202901.
[15] L. Zhang, X. Ren, Phys. Rev. B 71 (17) (2005) 174108.
[16] L. X. Zhang, X. B. Ren, Phys. Rev. B 73 (9) (2006) 094121.
[17] R. A. Eichel, P. Erhart, P. Träskelin, K. Albe, H. Kungl, M. J. Hoffmann, Phys. Rev. Lett. 100 (2008) 095504.
[18] R. R. Garipov, J. M. Spaeth, D. J. Keeble, Phys. Rev. Lett. 101 (24) (2008) 247604.
[19] H. Mestric, R.-A. Eichel, K.-P. Dinse, A. Ozarowski, J. van Tol, L. Brunel, J. Appl. Phys. 96 (12) (2004) 7440–7444.
[20] H. Meštrić, R. A. Eichel, K. P. Dinse, A. Ozarowski, J. van Tol, L. C. Brunel, H. Kungl, M. J. Hoffmann, K. A. Schönau, M. Knapp, H. Fuess, Phys. Rev. B 73 (18) (2006) 184105.
[21] H. Meštrić, R.-A. Eichel, T. Kloss, K.-P. Dinse, S. Laubach, S. Laubach, P. C. Schmidt, K. A. Schönau, M. Knapp, H. Ehrenberg, Phys. Rev. B 71 (2005) 134109.
[22] P. Erhart, R.-A. Eichel, P. Träskelin, K. Albe, Phys. Rev. B 76 (17) (2007) 174116.
[23] M. Iwata, N. Iijima, Y. Ishibashi, Ferroelectrics 428 (1) (2012) 1–7.
[24] D. J. Keeble, M. Loyo-Menoyo, Z. I. Y. Booq, R. R. Garipov, V. V. Eremkin, V. Smotrakov, Phys. Rev. B 80 (1) (2009) 014101.
[25] S. Pöykkö, D. Chadi, Phys. Rev. Lett. 83 (6) (1999) 1231–1234.
[26] E. Cockayne, B. P. Burton, Phys. Rev. B 69 (2004) 144116.
[27] E. Erdem, H. Kungl, M. J. Hoffmann, A. Ozarowski, J. V. Tol, L. C. Brunel, A. Ferroelectric, IEEE transactions on ultrasonics, ferroelectrics, and frequency control 55 (5) (2008) 1061–1068.
[28] X. Ren, Nature Mater. 3 (2004) 91–94.
[29] P. Erhart, P. Träskelin, K. Albe, Phys. Rev. B 88 (2013) 024107.
[30] R. Merkle, J. Maier, Phys. Chem. Chem. Phys. 5 (11) (2003).
[31] M. Schie, R. Waser, R. A. De Souza, J. Phys. Chem. C, 118 (2014) 15185-15192.
[32] R.-A. Eichel, E. Erünal, M. D. Drahus, D. M. Smyth, J. van Tol, J. Acker, H. Kungl, M. J. Hoffmann, Phys. Chem. Chem. Phys. 11 (2009) 8698–8705.
[33] D. Smyth, Ann. Rev. Mat. Sci. 15 (1985) 329–357.
[34] C.L. Freeman, J.A. Dawson, H.-R. Chen, J.H. Harding, L.B. Bin, D.C. Sinclair, J. Mater. Chem. 21, (2011) 4861–4868.
[35] M.S. Islam, Solid State Ionics 154-155 (2002) 75–85.
[36] M.S. Islam, J. Mater. Chem. 10 (2000) 1027–1038.
[37] E. Rauls, T. Frauenheim, Phys. Rev. B 69 (15) (2004) 155213.
[38] S. A. Centoni, B. Sadigh, G. H. Gilmer, T. J. Lenosky, T. Diaz de la Rubia, C. B. Musgrave, Phys. Rev. B 72 (2005) 195206.
[39] P. Erhart, K. Albe, A. Klein, Phys. Rev. B 73 (20) (2006) 205203.
[40] P. Erhart, K. Albe, J. Appl. Phys. 102 (08) (2007) 084111.
[41] P. Erhart, K. Albe, J. Appl. Phys. 104 (4) (2008) 044315.

[42] P. Erhart, D. Åberg, B. W. Sturm, K. Wu, V. Lordi, Appl. Phys. Lett. 97 (14) (2010) 142104.
[43] G. Kresse, J. Hafner, Phys. Rev. B 47 (1) (1993) 558–561.
[44] G. Kresse, J. Hafner, Phys. Rev. B 49 (20) (1994) 14251.
[45] G. Kresse, J. Furthmüller, Phys. Rev. B 54 (1996) 11169.
[46] G. Kresse, J. Furthmüller, Comput. Mater. Sci. 6 (1) (1996) 15–50.
[47] P. E. Blöchl, Phys. Rev. B 50 (24) (1994) 17953–17979.
[48] G. Kresse, D. Joubert, Phys. Rev. B 59 (3) (1999) 1758 – 1775.
[49] S. B. Zhang, J. E. Northrup, Phys. Rev. Lett. 67 (17) (1991) 2339–2342.
[50] S. Lany, A. Zunger, Phys. Rev. B 78 (23) (2008) 235104.
[51] P. Erhart, A. Klein, D. Åberg, B. Sadigh, Phys. Rev. B 90 (2014) 035204.
[52] Z. Zhang, P. Wu, L. Lu, C. Shu, Appl. Phys. Lett. 92 (11) (2008) 112909.
[53] J. Heyd, G. E. Scuseria, M. Ernzerhof, J. Chem. Phys. 118 (18) (2003) 8207–8215, erratum: *ibid.* **124**, 219906 (2006).
[54] F. Fuchs, J. Furthmüller, F. Bechstedt, M. Shishkin, G. Kresse, Phys. Rev. B 76 (11) (2007) 115109.
[55] C. Kittel, Introduction to Solid State Physics, 8th Edition, Wiley, New York, 2004.
[56] D. R. Lide, CRC Handbook of Chemistry and Physics, CRC Press, New York, 1998.
[57] A. Every, A. McCurdy, Landolt-Börnstein: numerical data and functional relationships in science and technology, New Series, Vol. III/29A, Springer, Heidelberg, 1992.